2D Effects Enhance Precision of Gradient-Based Tissue Patterning

Yuchong Long[1], Roman Vetter[1, 2], and Dagmar Iber[1, 2, *]

[1] *Department of Biosystems Science and Engineering, ETH Zürich, Mattenstrasse 26, 4058 Basel, Switzerland*
[2] *Swiss Institute of Bioinformatics, Mattenstrasse 26, 4058 Basel, Switzerland*

March 13, 2023

Robust embryonic development requires pattern formation with high spatial accuracy. In epithelial tissues that are patterned by morphogen gradients, the emerging patterns achieve levels of precision that have recently been explained by a simple one-dimensional reaction-diffusion model with kinetic noise. Here, we show that patterning precision is even greater if transverse diffusion effects are at play in such tissues. The positional error, a measure for spatial patterning accuracy, decreases in wider tissues but then saturates beyond a width of about ten cells. This demonstrates that the precision of gradient-based patterning in two- or higher-dimensional systems can be even greater than predicted by 1D models, and further attests to the potential of noisy morphogen gradients for high-precision tissue patterning.

Keywords: patterning, precision, morphogen gradient, reaction-diffusion model, 2D
[*] **Correspondence:** dagmar.iber@bsse.ethz.ch

Introduction

Morphogen gradients encode positional information to guide tissue patterning during embryonic development [1]. In the French flag model of patterning, morphogen concentration levels determine tissue domains of different cell fates [2]. While development is highly reproducible, reported gradient shapes differ substantially between embryos [3–7]—a seemingly contradictory situation. How a high patterning precision is achieved in spite of considerable noise in morphogen kinetics is therefore an active field of research. The problem has been studied intensely, both theoretically and experimentally [3, 4, 8–11, 7, 12–16], and recently gained new traction with the realization that morphogen gradients may be considerably more precise than previously measured [17–19].

Early theoretical models assumed a linear gradient shape [2, 20], but measurements of a wide range of morphogen gradients have since demonstrated that most morphogen gradients are better approximated by an exponential function,

$$C(x) = C_0 e^{-x/\lambda}, \tag{1}$$

with gradient amplitude C_0 and characteristic gradient length λ [4, 21, 22, 6, 7] (Fig. 1A). The position of patterning domain boundaries, herein termed the readout position,

$$x_\theta = \lambda \ln \frac{C_0}{C_\theta},$$

is located where the morphogen concentration reaches a threshold value $C(x_\theta) = C_\theta$. Due to molecular noise, the gradient shapes vary between embryos, and fitted exponential profiles vary in their parameters λ and C_0 [4, 5, 7, 17] such that the concentration threshold is reached at different readout positions in different embryos. This results in a positional error that can be quantified as the standard deviation of the readout position,

$$\sigma_x = \mathrm{stddev}[x_\theta]. \tag{2}$$

On the experimental side, most precision measurements have been carried out for the Bicoid (Bcd) gradient in the early *Drosophila* embryo [4], the Decapentaplegic (Dpp) gradient in the *Drosophila* wing disc [21, 5, 22], and Sonic Hedghehog (SHH) in the mouse neural tube [6, 7, 23]. Strikingly, in all patterning systems studied so far, the readout has been reported to be more precise than the gradients [4, 5, 7]. As a result, there has been a quest for precision-enhancing mechanisms. Spatio-temporal averaging of the morphogen concentration [4], simultaneous readout of opposing gradients [7], cell sorting [24], intermittent signaling in the *Drosophila* notum [25], and triggered self-organization in the Bcd gradient [26] have been suggested to increase gradient and readout precision. At least in the mouse neural tube, the positional error of the morphogen gradients has been overestimated [7, 17]. When corrected, the gradients are sufficiently precise to pattern the mouse neural tube. But how are such high levels of gradient precision achieved in spite of inevitable molecular noise?

In order to analyze how molecular noise translates into gradient variability, and how the various mechanisms described above would impact precision, we previously developed a numerical framework to generate and statistically evaluate noisy morphogen gradients. An exponential gradient shape can arise from a simple 1D reaction-diffusion model with diffusion coefficient D, production at rate p in the source, and linear degradation at rate d:

$$\frac{\partial C}{\partial t} = D \frac{\partial^2 C}{\partial x^2} + p\, H(-x) - d\, C, \tag{3}$$

where $H(x)$ is the Heaviside step function, limiting morphogen secretion to the source domain $x < 0$ (Fig. 1A). As a result of molecular noise, the kinetic parameters p, d, D will vary from cell to cell. For the reported physiological amount of parameter variability, the resulting 1D gradients differ between separate realizations (i.e., between embryos) (Fig. 1A), and have a positional error similar to that observed for the readouts in the mouse neural tube [17]. The previous analysis of 1D gradients further revealed that a small average cell diameter along the patterning axis is of key importance [18], potentially explaining why epithelia that are patterned by gradients, such as the neuroepithelium, are pseudostratified [27].

We wondered whether there would be additional effects at play that further reduce the variability of morphogen gradients. Spatio-temporal averaging over the cell surface has only minor effects on the precision of the gradient readout [18]. As a consequence, cilia and cell surface receptors can be expected to achieve a similar readout precision. Self-enhanced decay has

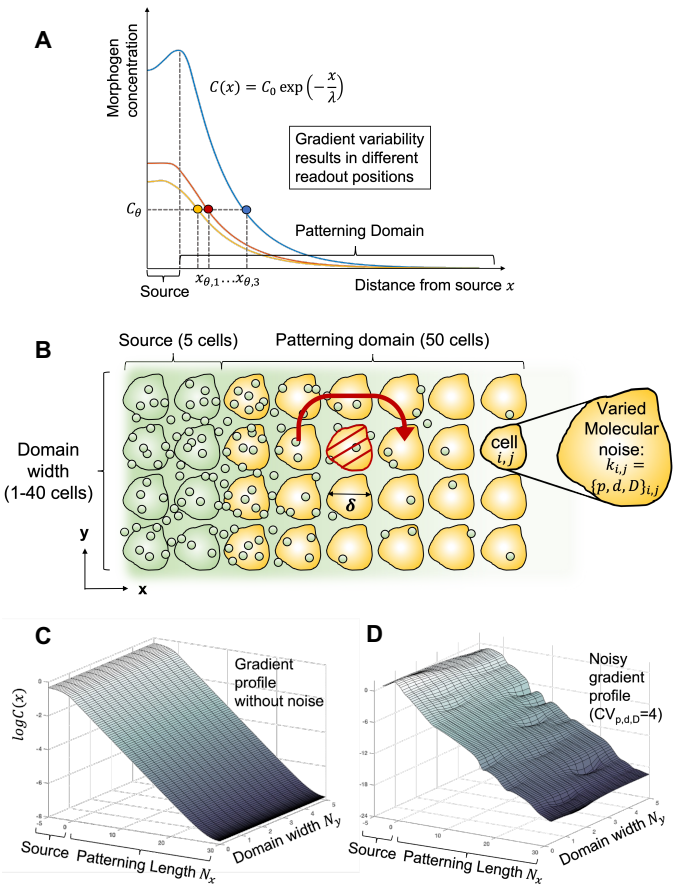

Fig. 1: Molecular noise induces variability in gradient shape and readout positions. A Inter-cellular and inter-embryonic variability in the morphogen production, decay and diffusion rates leads to differently shaped gradients (colors), which attain a concentration threshold C_θ at different readout positions $x_{\theta,1} \ldots x_{\theta,3}$. Their standard deviation is termed the positional error. **B** Morphogen diffusion in a two-dimensional tissue. Morphogens (small circles) are produced in the source (green), then secreted to the patterning domain (yellow). In 2D, morphogens can diffuse in both x and y directions, allowing them to bypass malfunctioning cells (red). In 1D, such cells have a greater impact on the gradient shape, effectively acting as transport barriers that let the morphogen concentration drop to zero beyond. **C,D** Simulated morphogen gradients on a 2D domain, without (C) and with molecular noise (D). The morphogen concentration $C(x, y)$ is plotted on a logarithmic scale, and a kinetic cell-to-cell variability of $\mathrm{CV}_{p,d,D} = 4$ (coefficient of variation) is used for illustration purposes. Cells with poor transport capabilities result in local dips in the gradient profile.

been suggested to increase gradient robustness to noise in the morphogen source [28], but this effect is negligible when considering the effects of molecular noise more explicitly [19]. One aspect, however, has not been analyzed systematically: That of tissue dimensionality. After all, tissues are three-dimensional, and patterning domains are at least two-dimensional, even if morphogen sensing is restricted to the apical surface, as seems to be the case for SHH in the neural tube as its receptor PTCH1 is restricted to a cilium located on the apical surface [29]. One-dimensional domain approximations are known to overestimate the variability of gradients as morphogens can bypass defective cells in 2D and 3D [5] (Fig. 1B). How this effect translates into the spatial accuracy of patterning, and how it depends on the width of the patterning domain has, however, not been studied.

By extending our stochastic gradient analysis to 2D tissues (Fig. 1B-D), we now find that the readout precision and the robustness of gradient shape are further enhanced if transverse diffusion effects are considered. We show that the positional error decreases as the tissue widens, but then saturates as the width reaches about ten cells. Our findings provide further evidence that noisy morphogen gradients are able to guide high-precision tissue patterning, and offer a reason why certain developing tissues may favor a specific dimension over another in the context of patterning precision.

Results

A 2D model for cellular tissue patterning

We approximate the cellular tissue with a regular rectangular 2D lattice of length L_x and width L_y, such that patterning occurs along the x-axis. The lattice represents a 2D patch of cells of diameter δ each, which determines the domain length $L_x = N_x\delta$ and width $L_y = N_y\delta$, given the number of cells N_x and N_y in x and y direction (Fig. 1B–D). We ignore variability in cell areas or diameters here, as physiological levels were previously shown to have negligible impact on gradient precision [18]. The patterning axis of length L_x is further divided into a morphogen source $[-L_\mathrm{s}, 0]$ and a patterning domain $[0, L_\mathrm{p}]$, such that $L_x = L_\mathrm{s} + L_\mathrm{p}$. The steady-state reaction-diffusion equation from 1D (Eq. 3) is extended to 2D by writing

$$\frac{\partial C}{\partial t} = 0 = D\left(\frac{\partial^2 C}{\partial x^2} + \frac{\partial^2 C}{\partial y^2}\right) + p\,H(-x) - d\,C. \qquad (4)$$

We solved Eq. 4 numerically (see Methods for details), with two sets of boundary conditions: 1) zero-flux boundary conditions on all four sides of the domain, and 2) periodic boundary conditions in y direction and zero-flux boundary conditions in x direction. The latter is to mimic an infinitely wide domain and to minimize the finite size effects that result from the choice of specific boundary conditions in y.

Gradients are more robust in wider tissues

The 2D solution can be viewed as an ensemble of gradients along each cell row. For a patterning domain with N_y cells in width, Eq. 1 can be fitted to each of the N_y gradients. The variability in the gradient parameters λ and C_0 is then quantified by the coefficient of variation $\mathrm{CV}_\lambda = \sigma_\lambda/\mu_\lambda$ and $\mathrm{CV}_0 = \sigma_{C_0}/\mu_{C_0}$. As the number of cells orthogonal to the patterning axis, N_y, increases from 1 to 40, our stochastic gradient analysis shows that the variability of λ and C_0 is inversely proportional to the square root of N_y (Fig. 2A,B,E,F):

$$\mathrm{CV}_\lambda(N_y) = \frac{a_\lambda}{\sqrt{N_y}} + \mathrm{CV}_\lambda(\infty),$$

$$\mathrm{CV}_0(N_y) = \frac{a_0}{\sqrt{N_y}} + \mathrm{CV}_0(\infty).$$

Specifically, under zero-flux boundary conditions and with a physiological amount of cell-to-cell kinetic variability (Methods), $a_\lambda = 0.0294 \pm 0.0004$, $\mathrm{CV}_\lambda(\infty) = (9.96 \pm 1.91) \times 10^{-4}$, $a_0 = 0.2113 \pm 0.0026$ and $\mathrm{CV}_0(\infty) = 0.0028 \pm 0.0012$ as determined by curve-fitting (bounds are standard errors). This square-root relation can be explained by the Law of Large Numbers. The constants $\mathrm{CV}_\lambda(\infty)$ and $\mathrm{CV}_0(\infty)$ indicate the saturation of the variability as the domain width reaches infinity. The gradient variability parameters CV_λ and CV_0 decrease significantly as the tissue width reaches about ten cells, before the gradient variability gradually flattens (Fig. 2A,B).

Our findings echo with Bollenbach et al. [5] in that 2D tissues weaken the effect of deficient cells on morphogen concentration,

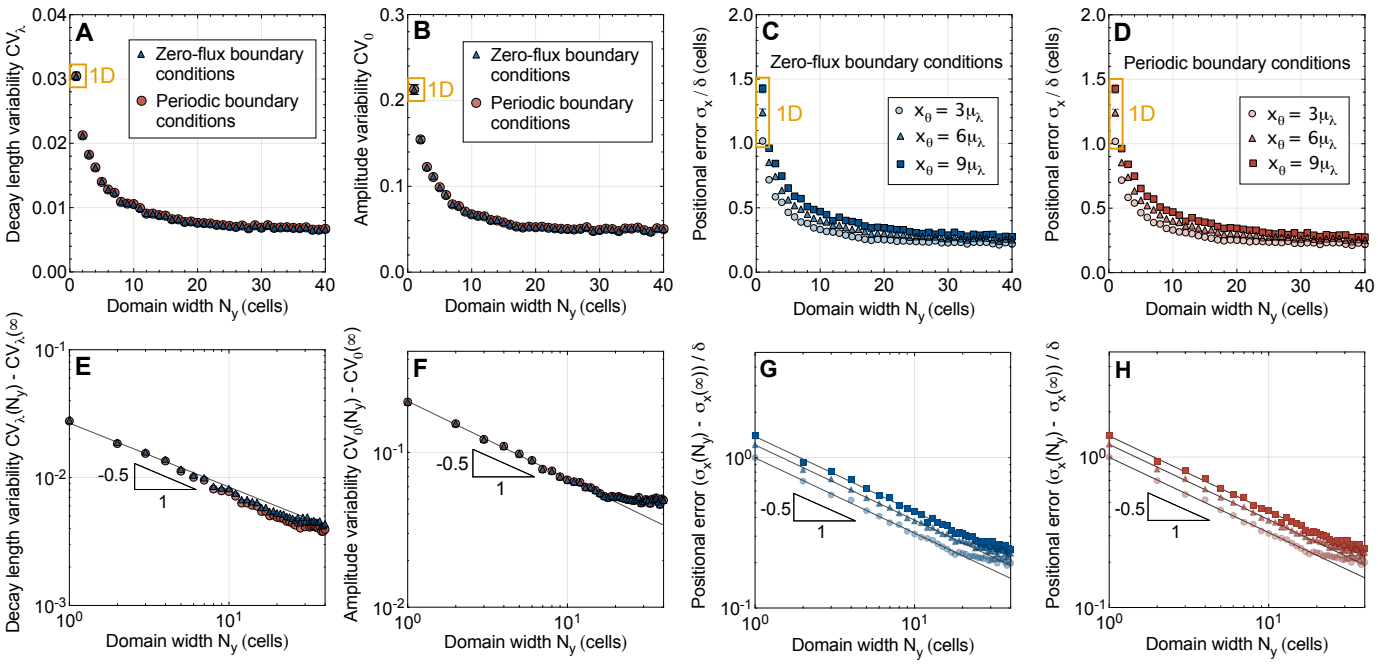

Fig. 2: Impact of domain width on gradient variability and readout precision. Statistical evaluation of $n = 1000$ numerically generated, noisy morphogen gradients with cell-to-cell variability in the kinetic parameters $k = p, d, D$ defined by a coefficient of variation $\mathrm{CV}_k = 0.3$. The gradient variability and positional errors were calculated at a single cell-row at the middle of the domain (i.e., at $y = L_y/2$). Error bars are SEM, but are mostly smaller than the symbols. Generated 2D gradients with a single cell row ($N_y = 1$, orange) are identical to 1D gradients within statistical errors. **A,B** Gradient variability, as measured by the coefficients of variation for the gradient decay length (CV_λ) and amplitude (CV_0) as a function of the domain width. Results for zero-flux (blue triangles) and periodic (red circles) BCs are nearly equal. **C,D** Positional error in units of cell diameters, measured at three different readout positions along the patterning axis (different symbols), as a function of the domain width, for zero-flux (C, blue) and periodic tissue boundaries (D, red). **E–H** Log-log plots of A–D reveal the square-root scaling of gradient variability and of the positional error with the domain width. Solid lines are fitted relationships of the form $Y(N_y) - Y(\infty) = a/\sqrt{N_y}$. Deviation from the square-root scaling sets in as L_y exceeds a certain width (see also Supplemental Figs. S1 and S2).

thus lowering the concentration uncertainty. From this point of view, the wider the tissue, the larger the set of diffusion paths morphogens can choose from to bypass deficient cells, at the cost of a longer path to travel. Increasingly long detours gradually weaken this compensatory effect, such that the benefit of even wider tissues tends to zero. More generally, diffusion in y smooths out local fluctuations by allowing the noise experienced by one gradient to disperse among its neighbors, which is otherwise harder to achieve in 1D. Indeed, the gradient variability in wider tissues is considerably lower than that predicted in 1D (marked in orange in Fig. 2A–D) [17, 18].

Patterning precision increases in wider tissues

Not only gradient variability is reduced, but also the spatial accuracy they convey to the patterned cells is enhanced in wider tissues (Fig. 2C,D,G,H). Similar to the scaling of gradient variability with respect to the domain width, the positional error is inversely proportional to the square root of the domain width:

$$\frac{\sigma_x(N_y) - \sigma_x(\infty)}{\delta} = \frac{a_x}{\sqrt{N_y}}. \tag{5}$$

The further away from the morphogen source, the larger the positional error [5, 17, 18], an effect that we also observe here in 2D. Nevertheless, our gradient quantifications revealed that even for a readout position as far as $x_\theta = 9\mu_\lambda$ (where $\mu_\lambda = 4\delta$ is the average gradient decay length), the positional error is significantly reduced in wider domains. Eq. 5 holds independent from the position in the pattern (Fig. 2), and regardless of the boundary conditions.

In Eq. 5, we non-dimensionalized the positional error by the constant cell diameter δ to provide some intuition for the patterning precision relative to the size of the cells. Remarkably, extending the tissue width from one to two cells is sufficient to bring the positional error to subcellular levels even at the readout position furthest from the source, $x_\theta = 9\mu_\lambda$, and in wider domains it can go considerably lower still. Specifically, for a nearly square tissue with 50 cells along the patterning axis and 40 cells, the positional error at $x_\theta = 3\mu_\lambda$ is reduced to less than a fourth of a cell diameter ($\sigma_x/\delta = 0.22$). With a readout position far away from the source, i.e. at $x_\theta = 9\mu_\lambda$, the positional error is still reduced to 28% of one cell diameter.

In the generation of these gradients, we fixed the cell diameter $\delta = 5\,\mu\mathrm{m}$. Similar behavior is observed with larger and smaller cells, the only qualitative difference being that the deviation sets in at different number of cell rows N_y, but at approximately equal domain widths $L_y = N_y\delta$ (Supplemental Figs. S1 and S2). Moreover, we determined the gradient variability and positional error in the middle of the domain width, at $y = L_y/2$, in Fig. 2. The results are unchanged if averaged over the entire width, as may be more relevant for robust development, except that the square-root scaling (Eq. 5) is found to hold even more robustly, over the entire range of tested tissue widths (Supplemental Fig. S3).

Patterning precision increases with narrower cells

In the mouse neural tube, cells are longer along the body axis than in the dorsal-ventral direction [30], along which patterning via SHH and BMP gradients occurs. We therefore relaxed the

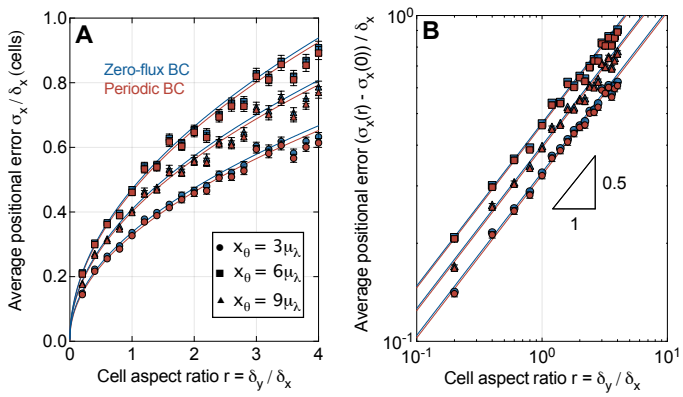

Fig. 3: Effect of cell aspect ratio on patterning precision. **A** When cells have a diameter of δ_x along the patterning axis and δ_y in transverse direction, patterning precision increases with narrower cells (larger aspect ratio). **B** Log-log plot of the data shown in A, revealing a square-root scaling $\sigma_x/\delta_x \sim \sqrt{\delta_y/\delta_x}$. Data points indicate mean ± SEM from $n = 1000$ independent gradient realizations at fixed $\delta_x = \mu_\lambda/4$ and varied δ_y. Different symbols represent different readout positions along the patterned axis. Solid lines are fitted square-root relationships.

previous assumption that cells have the same diameter δ in both tissue directions, and tested how the readout precision would be affected by the cell aspect ratio $r = \delta_x/\delta_y$, defined as the ratio between the cell diameters along the patterning axis and orthogonal to it. As the aspect ratio increases, i.e., as the cells become wider in the transverse direction, the positional error increases (Fig. 3). We observe that the cell aspect ratio affects the positional error, now a function of both cell diameters δ_x and δ_y, as

$$\frac{\sigma_x(\delta_x, \delta_y) - \sigma_x(\delta_x, 0)}{\delta_x} \propto \sqrt{\frac{\delta_y}{\delta_x}}. \tag{6}$$

Since the one-dimensional positional error is asympotically proportional to the square root of the cell diameter in patterning direction ($\sigma_x(\delta_x, 0) \sim \sqrt{\delta_x \mu_x}\mu_\lambda/L_\mathrm{s}$) [18], Eq. 6 can be rearranged into

$$\sigma_x \sim \sqrt{\delta_x}\left(\sqrt{\delta_y} + \sqrt{l}\right), \tag{7}$$

where

$$l \sim \mu_x \left(\frac{\mu_\lambda}{L_\mathrm{s}}\right)^2$$

is an asymptotic length scale independent of the cell diameters δ_x and δ_y. This length scale does, however, depend on a number of other factors, such as the mean characteristic gradient length μ_λ, the mean position μ_x in the patterning domain where the morphogen gradient is read out, and the size of the morphogen source L_s. Via the proportionality prefactor, it will also depend on the type of 2D cell arrangement (here a rectangular array for simplicity), the morphogen sensing strategy employed by the cells [18] (here concentration averaging over the cell area), and possibly mildly on other factors like the non-uniformity of cell sizes or the precise nature of the variability in the kinetic parameters. Since the average gradient decay length is given by $\mu_\lambda \approx \sqrt{D/d}$ for physiological values of kinetic variability ($\mathrm{CV}_{d,D} \lesssim 0.5$) [17], this asymptotic length scale can be rewritten as

$$l \sim \frac{\mu_x}{L_\mathrm{s}^2}\frac{D}{d}. \tag{8}$$

Thus, in summary, the absolute positional error carried by morphogen gradients in a two-dimensional patterning scenario with kinetic cell-to-cell variability is lower if cells are narrower not only along the direction of the gradient, but also if they are narrower in the transverse direction (Eq. 7). This can intuitively be understood from the smoothing effect that transverse diffusion has on morphogen levels. However, this takes effect only when nearby parallel gradients differ locally, and so the impact of the cell size orthogonal to the patterning direction is weaker than parallel to it. Mathematically, this is manifest in Eq. 7 in the offset $\sqrt{l}$, which lets the cell width δ_y impact on the positional error only if is is sufficiently large in comparison to l. By virtue of Eq. 8, this will be the case near the morphogen source (small μ_x), in tissues with a large source (large L_s), for slow diffusion (small D), and quick degradation (large d). The offset $\sqrt{l}$ in this relationship potentially explains why it is tolerable in the developing neural tube for cells to be wider along the anterior-posterior axis than in the dorsal-ventral direction, along which the neuroepithelium is patterned into different progenitor domains.

Patterning precision in the *Drosophila* wing disc

Our findings bear the potential to explain patterning precision not only in vertebrate development. In the *Drosophila* wing disc (Fig. 4A), the Dpp gradient defines the positions of the longitudinal veins. Strikingly, Dpp readout positions remain at the same relative location in the domain despite substantial tissue growth, a phenomenon that is referred to as pattern scaling [22, 31]. The position of the anterior Spalt domain boundary, which places the L2 vein, remains at 40–45% of the anterior domain length [32, 5, 31]. Scaling of the readout with the length of the patterning domain is achieved by the parallel increase in the gradient amplitude and length [22, 33]. We previously showed that the positional error remains largely constant in spite of the growing absolute readout distance from the source and the expanding gradient length, because the parallel increase in the source width and decrease in the average apical cell areas [34–36, 22, 37] compensate according to $\sigma_x \sim \sqrt{\delta\mu_x}\mu_\lambda/L_\mathrm{s}$ [18]. While the predicted positional error at $\mu_x/L_\mathrm{p} = 0.4$ remains below about 4 µm when considering a 1D domain [18] (Fig. 4B, green), this still corresponds to more than two cell diameters. With a domain that is $N_y = 10$ cells in width—a number easily surpassed in the wing pouch—we find a positional error well below a single cell diameter throughout development (Fig. 3B, orange), a more-than-3-fold reduction compared to the 1D perspective. These observations suggest that 2D effects are key to ensuring high patterning precision in tissue development.

Discussion

Molecular noise has long been believed to cause large variability during embryonic development. This has started to change recently, and our present findings underpin this trend. By statistically analyzing the effect of molecular noise on morphogen concentration gradients, we show that for realistic morpho-kinetic noise levels, positional information can be expected to be conveyed to cells in two-dimensional tissues with sub-cellular resolution. While our study builds on recently developed modeling ideas [17, 18], a new perspective was required to arrive at this result: Tissue patterning typically occurs in at least two dimensions, and morphogens can diffuse also orthogonal to the patterning axis. Not only does this allow them to bypass malfunctioning cells [5]. Transverse diffusion also substantially smoothens out local morphogen fluctuations in the entire tissue, leading to a considerable drop in gradient variability and in the positional error.

We found that patterning precision scales with the square root of the number of cells along the tissue width—an intuitive relationship with theoretical roots in statistics. Arriving at this

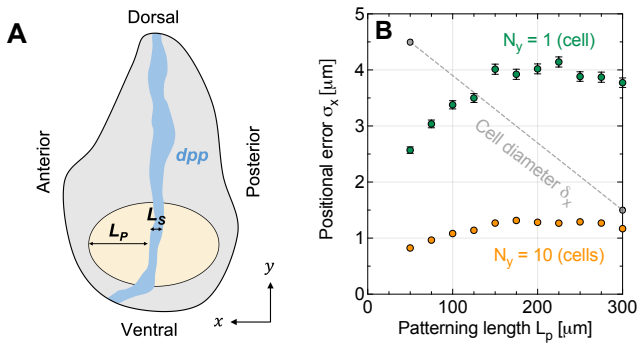

Fig. 4: Effect of tissue width on patterning precision in the *Drosophila* wing disc. A Schematic illustration of the wing disc (gray) with its Dpp source along the anterior-posterior boundary (blue). The tissue width orthogonal to the Dpp gradient is in dorsal-ventral direction. The wing pouch is shown in beige. **B** Evolution of the predicted positional error of the Dpp gradient as the wing pouch widens over time, at $\mu_x = 0.4L_\mathrm{p}$ for $\mu_\lambda = 0.11L_\mathrm{p}$, $L_\mathrm{s} = 0.16L_\mathrm{p}$, and $\delta_x = 5.1\,\mu\mathrm{m} - 0.012L_\mathrm{p}$ [18]. When the tissue width is accounted for by 10 cell rows ($N_y = 10$, orange), the positional error is substantially lower than with only one cell row ($N_y = 1$, green), and remains well below once cell diameter (gray dashed line). Data points indicate mean ± SEM from $n = 1000$ independent gradients.

result required extending the previous 1D model for patterning to two dimensions. A striking consequence of this relationship is that even a few cells across are sufficient to allow morphogen-sensing cells to differentiate according to their location in the pattern with a positional accuracy below a single cell diameter. Compared to 1D patterning scenarios, 2D morphogen transport allows for a considerable precision enhancement up to a tissue width of roughly ten cells, before saturation sets in. This gain can be as big as 3- to 4-fold. The precision-enhancing 2D effects observed here are not limited to a close vicinity of the morphogen source, but they apply anywhere in the tissue, also in regions distal from the source. Our data suggests that high-precision tissue patterning with morphogen gradients is possible in spite of molecular and biological variability also far away from the origin.

Our work also reveals how gradient variability depends on the cell aspect ratio, providing a potential explanation for the biased cell shape in the developing neural tube [30]. Although patterning precision increases when cells are narrower in both tissue directions, the benefit is greater along the patterning axis (Eq. 7). For robust patterning, cells that are wider perpendicular to the gradient than parallel to it are more tolerable. This may equip Nature with a tunable degree of freedom that can be tailored to a required level of developmental precision—a hypothesis that could be amenable to experimental testing, and which could be relevant for gradient-based tissue engineering. Our findings also hint at a developmental advantage for widening tissues, as long as their cells do not widen with it. What brings down the positional error is the number of cells across the tissue, N_y, not the width itself, L_y. These results put our previous analysis on the effect of cell size on patterning precision [18] into a broader context. In the *Drosophila* eye disc, the initial size at 40 h after hatching is about $[L_x, L_y] = [50, 100]$ µm [38]. With an apical area of 7 µm^2 and smaller [35], 100 µm corresponds to at least $N_y = 60$ cells in width. We now find that for such tissues, the positional error is reduced by about 4-fold compared to the traditional 1D perspective. For larger number of cells, the precision-enhancing effect, however, plateaus. Francis Crick started his seminal paper on the role of diffusion in gradient patterning by quoting Lewis Wolpert, "It has been a great surprise and of considerable importance to find that most embryonic fields seem to involve distances of less than 100 cells, and often less than 50." [20]. In light of our work, such tissue widths appear sufficient for precise patterning.

Although we linked the implications of 2D diffusion for patterning precision to two specific epithelial tissues—the vertebrate neuroepithelium and the fly wing disc—the main results presented here are system-agnostic, and might underlie developmental precision across species more generally. As with all theoretical and modeling work, our predictions from a statistical analysis of synthetically generated noisy morphogen gradients requires experimental validation, which we hope to motivate herewith. An open question is the impact of complex tissue architecture, such as that of pseudostratified epithelia [39], on patterning precision [27]. In light of our study, it appears plausible that the densely packed cells with stratified nuclei can help buffer morphogen level fluctuations similar to the stratified cell rows in our 2D cell arrays here, at least for morphogens that are sensed along the lateral sides of cells, such as Bone Morphogenetic Protein (BMP) in the neural tube [40]. Our results would then suggest that the positional error cells experience from reading out the BMP gradient is reduced by the strong pseudostratification. Generally, one may ask if (and to which degree) patterning precision can be further enhanced in three-dimensional tissues, a question that we leave for future research. While our model is straightforward to generalize to 3D, previous results by Bollenbach et al. [5] hint at an affirmative answer.

Finally, a few potential limitations of our model deserve being mentioned. While our statistical approach to generate noisy morphogen gradients is among the ones with the most detailed representation of molecular noise in the literature, there can be a range of other sources of biological variability involved in tissue patterning processes that were not represented here. Noise in the molecular readout mechanism, in regulatory interactions (either during the formation of the morphogen gradient or downstream), or in the fate decision process, are some of them. We restricted our analysis of spatial precision to the pure gradients here. Moreover, our analysis is based on a representation of the morphogen concentration as a continuous function $C(x, y)$, ignoring the discrete, particulate nature that may become relevant at low morphogen numbers. We also assumed isotropic morphogen transport properties within the 2D tissue plane for simplicity. Variability in the cell areas, on the other hand, would not be expected to alter our findings [18], although it may be of interest to extend the present model from a rectangular cell grid to more realistic tissue geometries with irregular cell arrangements.

Methods

Generation of 2D morphogen gradients from molecular noise. To study the inter-embryonic variability and intra-embryonic noisiness of morphogen gradients in a quantitative way, we generated large numbers of statistically independent gradients numerically. We discretized the 2D tissue domain $[-L_\mathrm{s}, L_\mathrm{p}] \times [0, L_y]$ into a rectangular grid (visible in Fig. 1C,D), using 3×3 grid points per cell as a good compromise between computational speed and numerical accuracy. For each cell at position i, j in the tissue, we drew random morpho-kinetic parameters p_{ij}, d_{ij}, D_{ij} from log-normal distributions analogous to previous 1D studies [17–19], such that the noisy exponential morphogen gradients $C(x, y)$ emerge as solutions of the 2D

steady-state reaction-diffusion problem

$$0 = D_{ij}\left(\frac{\partial^2 C(x,y)}{\partial x^2} + \frac{\partial^2 C(x,y)}{\partial y^2}\right) + p_{ij}\,H(-x) - d_{ij}\,C(x,y). \tag{9}$$

Each of the kinetic parameter distributions was defined by a mean value μ_k and a coefficient of variation $\mathrm{CV}_k = \sigma_k/\mu_k$ for $k = p, d, D$. Physiological molecular noise levels were identified previously [17], and we used the same value $\mathrm{CV}_k = 0.3$ here. We then solved Eq. 9 with the finite difference method, using a five-point central difference stencil, in Matlab 2021b. Zero-flux boundary conditions were imposed in x direction, and zero-flux or periodic boundaries were assumed in the width direction (y) as indicated in the figures. A relative error tolerance of 10^{-10} was used to terminate the iterative solver. Repeating this process with new random kinetic parameters for all cells yielded $n = 1000$ independent realizations of 2D morphogen concentration profiles (as shown exemplarily in Fig. 1C,D), which we then evaluated statistically.

Calculation of gradient variability. To extract the amount of variability in the gradient decay length and amplitude, we interpreted each of the n noisy 2D morphogen gradients $C(x, y)$ as an ensemble of N_y parallel gradients $C_j(x)$, each running along a row of cells in patterning direction. These gradients were approximately exponential along x, with a slight bend at the distal tissue boundary due to the imposed boundary conditions. Along the central cell row $j = N_y/2$ (or along all of them for Supplemental Fig. S3), we therefore fitted the deterministic solution [17]

$$C(x) = C_0 \frac{\cosh[(L_\mathrm{P} - x)/\lambda)]}{\cosh[L_\mathrm{P}/\lambda]}$$

to the noisy concentration profiles in the patterning domain, after logarimizing them first. Repeating this process for all n 2D gradients yielded a set of gradient decay lengths $\{\lambda_1, ..., \lambda_n\}$ and amplitudes $\{C_{0,1}, ..., C_{0,n}\}$, from which we computed the coefficients of variation, CV_λ and CV_0. Standard errors were determined using bootstrapping.

Statistical evaluation of readout positions and patterning precision. We used spatial averaging over the cell surfaces to determine the morphogen concentration each cell is exposed to—a choice that does not affect the positional information conveyed to the cells significantly [18]. With the resulting concentration profiles in the form of step functions, we determined the positional error according to its definition, as the standard deviation of the locations where the gradients attain a threshold value (Eq. 2). Since 2D gradients are not always monotonic, there can be multiple such locations along a single gradient. In such cases, we used their mean location to define the readout position x_θ. At three different such (average) readout positions $x_\theta = 3\mu_\lambda, 6\mu_\lambda, 9\mu_\lambda$, we evaluated their standard deviations over the $n = 1000$ noisy gradients. Standard errors were then again calculated using bootstrapping.

Code Availability

The source code is released under the 3-clause BSD license. It is available as a public git repository at `https://git.bsse.ethz.ch/iber/Publications/2023_long_2d_precision`.

Acknowledgements

This work was partially funded by the Swiss National Science Foundation under Sinergia grant CRSII5_170930.

Competing Interests

The authors declare that they have no competing interests.

Author Contributions

Conceptualization, R.V. and D.I.; Software & Simulations, Y.L. and R.V.; Formal Analysis, R.V.; Supervision, R.V. and D.I.; Visualization, Y.L.; Writing, R.V., D.I., and YL.; Funding Acquisition, D.I.

References

[1] K. W. Rogers and A. F. Schier. Morphogen Gradients: From Generation to Interpretation. *Annu. Rev. Cell Dev. Biol.*, 27:377–407, 2011. doi: 10.1146/annurev-cellbio-092910-154148.

[2] L. Wolpert. Positional information and the spatial pattern of cellular differentiation. *J. Theor. Biol.*, 25:1–47, 1969. doi: 10.1016/S0022-5193(69)80016-0.

[3] B. Houchmandzadeh, E. Wieschaus, and S. Leibler. Establishment of developmental precision and proportions in the early *Drosophila* embryo. *Nature*, 415:798–802, 2002. doi: 10.1038/415798a.

[4] T. Gregor, D. W. Tank, E. F. Wieschaus, and W. Bialek. Probing the Limits to Positional Information. *Cell*, 130: 153–164, 2007. doi: 10.1016/j.cell.2007.05.025.

[5] T. Bollenbach, P. Pantazis, A. Kicheva, C. Bökel, M. González-Gaitán, and F. Jülicher. Precision of the Dpp gradient. *Development*, 135:1137–1146, 2008. doi: 10.1242/dev.012062.

[6] M. Cohen, A. Kicheva, A. Ribeiro, R. Blassberg, K. M. Page, C. P. Barnes, and J. Briscoe. Ptch1 and Gli regulate Shh signalling dynamics via multiple mechanisms. *Nat. Commun.*, 6:6709, 2015. doi: 10.1038/ncomms7709.

[7] M. Zagorski, Y. Tabata, N. Brandenberg, M. P. Lutolf, G. Tkačik, T. Bollenbach, J. Briscoe, and A. Kicheva. Decoding of position in the developing neural tube from antiparallel morphogen gradients. *Science*, 356:1379–1383, 2017. doi: 10.1126/science.aam5887.

[8] A. D. Lander, W.-C. Lo, Q. Nie, and F. Y. M. Wan. The Measure of Success: Constraints, Objectives, and Tradeoffs in Morphogen-mediated Patterning. *Cold Spring Harb. Perspect. Biol.*, 1:a002022, 2009. doi: 10.1101/cshperspect.a002022.

[9] Y. Morishita and Y. Iwasa. Accuracy of positional information provided by multiple morphogen gradients with correlated noise. *Phys. Rev. E*, 79:061905, 2009. doi: 10.1103/PhysRevE.79.061905.

[10] Y. Morishita and Y. Iwasa. Coding Design of Positional Information for Robust Morphogenesis. *Biophys. J.*, 101: 2324–2335, 2011. doi: 10.1016/j.bpj.2011.09.048.

[11] G. Tkačik, J. O. Dubuis, M. D. Petkova, and T. Gregor. Positional Information, Positional Error, and Readout Precision in Morphogenesis: A Mathematical Framework. *Genetics*, 199:39–59, 2015. doi: 10.1534/genetics.114.171850.

[12] T. Erdmann, M. Howard, and P. R. ten Wolde. Role of Spatial Averaging in the Precision of Gene Expression Patterns. *Phys. Rev. Lett.*, 103:258101, 2009. doi: 10.1103/PhysRevLett.103.258101.

[13] T. R. Sokolowski and G. Tkačik. Optimizing information flow in small genetic networks. iv. spatial coupling. *Phys. Rev. E*, 91:062710, 2015. doi: 10.1103/PhysRevE.91.062710.

[14] D. Ellison, A. Mugler, M. D. Brennan, S. H. Lee, R. J. Huebner, E. R. Shamir, L. A. Woo, J. Kim, P. Amar, I. Nemenman, A. J. Ewald, and A. Levchenko. Cell–cell

communication enhances the capacity of cell ensembles to sense shallow gradients during morphogenesis. *Proc. Natl. Acad. Sci. U.S.A.*, 113:E679–E688, 2016. doi: 10.1073/pnas.1516503113.

[15] A. Mugler, A. Levchenko, and I. Nemenman. Limits to the precision of gradient sensing with spatial communication and temporal integration. *Proc. Natl. Acad. Sci. U.S.A.*, 113:E689–E695, 2016. doi: 10.1073/pnas.1509597112.

[16] R. Reyes, A. Lander, and M. Nahmad. Dynamic readout of the Hh gradient in the Drosophila wing disc reveals pattern-specific tradeoffs between robustness and precision. *BioRxiv*, 2022. doi: 10.1101/2022.12.21.521489.

[17] R. Vetter and D. Iber. Precision of morphogen gradients in neural tube development. *Nat. Commun.*, 13:1145, 2022. doi: 10.1038/s41467-022-28834-3.

[18] J. A. Adelmann, R. Vetter, and D. Iber. Impact of cell size on morphogen gradient precision. *BioRxiv*, 2022. doi: 10.1101/2022.02.02.478800.

[19] J. A. Adelmann, R. Vetter, and D. Iber. Patterning precision under non-linear morphogen decay and molecular noise. *BioRxiv*, 2022. doi: 10.1101/2022.11.04.514993.

[20] F. Crick. Diffusion in embryogenesis. *Nature*, 225:420–422, 1970. doi: 10.1038/225420a0.

[21] A. Kicheva, P. Pantazis, T. Bollenbach, Y. Kalaidzidis, T. Bittig, F. Jülicher, and M. González-Gaitán. Kinetics of Morphogen Gradient Formation. *Science*, 315:521–525, 2007. doi: 10.1126/science.1135774.

[22] O. Wartlick, P. Mumcu, A. Kicheva, T. Bittig, C. Seum, F. Jülicher, and M. González-Gaitán. Dynamics of Dpp Signaling and Proliferation Control. *Science*, 331:1154–1159, 2011. doi: 10.1126/science.1200037.

[23] K. Exelby, E. Herrera-Delgado, L. Garcia Perez, R. Perez-Carrasco, A. Sagner, V. Metzis, P. Sollich, and J. Briscoe. Precision of Tissue Patterning is Controlled by Dynamical Properties of Gene Regulatory Networks. *Development*, 2021. doi: 10.1242/dev.197566.

[24] T. Y.-C. Tsai, M. Sikora, P. Xia, T. Colak-Champollion, H. Knaut, C.-P. Heisenberg, and S. G. Megason. An adhesion code ensures robust pattern formation during tissue morphogenesis. *Science*, 370:113–116, 2020. doi: 10.1126/science.aba6637.

[25] M. Cohen, M. Georgiou, N. L. Stevenson, M. Miodownik, and B. Baum. Dynamic Filopodia Transmit Intermittent Delta-Notch Signaling to Drive Pattern Refinement during Lateral Inhibition. *Dev. Cell*, 19:78–89, 2010. doi: 10.1016/j.devcel.2010.06.006.

[26] S. Surkova, A. V. Spirov, V. V. Gursky, H. Janssens, A.-R. Kim, O. Radulescu, C. E. Vanario-Alonso, D. H. Sharp, M. Samsonova, and J. Reinitz. Canalization of Gene Expression in the *Drosophila* Blastoderm by Gap Gene Cross Regulation. *PLOS Biol.*, 7:e1000049, 2009. doi: 10.1371/journal.pbio.1000049.

[27] D. Iber and R. Vetter. Relationship between epithelial organization and morphogen interpretation. *Curr. Opin. Genet. Dev.*, 75:101916, 2022. doi: 10.1016/j.gde.2022.101916.

[28] A. Eldar, D. Rosin, B.-Z. Shilo, and N. Barkai. Self-Enhanced Ligand Degradation Underlies Robustness of Morphogen Gradients. *Dev. Cell*, 5:635–646, 2003. doi: 10.1016/S1534-5807(03)00292-2.

[29] M. Saade, I. Gutiérrez-Vallejo, G. Le Dréau, M. A. Rabadán, D. G. Miguez, J. Buceta, and E. Martí. Sonic hedgehog signaling switches the mode of division in the developing nervous system. *Cell Rep.*, 4:492–503, 2013. doi: 10.1016/j.celrep.2013.06.038.

[30] V. Ribes, N. Balaskas, N. Sasai, C. Cruz, E. Dessaud, J. Cayuso, S. Tozer, L. L. Yang, B. Novitch, E. Marti, and J. Briscoe. Distinct Sonic Hedgehog signaling dynamics specify floor plate and ventral neuronal progenitors in the vertebrate neural tube. *Genes Dev.*, 24:1186–1200, 2010. doi: 10.1101/gad.559910.

[31] F. Hamaratoglu, A. M. de Lachapelle, G. Pyrowolakis, S. Bergmann, and M. Affolter. Dpp signaling activity requires Pentagone to scale with tissue size in the growing Drosophila wing imaginal disc. *PLoS Biol.*, 9:e1001182, 2011.

[32] M. A. Sturtevant, B. Biehs, E. Marin, and E. Bier. The spalt gene links the A/P compartment boundary to a linear adult structure in the Drosophila wing. *Development*, 124: 21–32, 1997.

[33] P. Fried and D. Iber. Dynamic scaling of morphogen gradients on growing domains. *Nat. Commun.*, 5:5077, 2014. doi: 10.1038/ncomms6077.

[34] T. Aegerter-Wilmsen, M. B. Heimlicher, A. C. Smith, P. B. de Reuille, R. S. Smith, C. M. Aegerter, and K. Basler. Integrating force-sensing and signaling pathways in a model for the regulation of wing imaginal disc size. *Development*, 139:3221–3231, 2012.

[35] D. Corrigall, R. F. Walther, L. Rodriguez, P. Fichelson, and F. Pichaud. Hedgehog signaling is a principal inducer of Myosin-II-driven cell ingression in *Drosophila* epithelia. *Dev. Cell*, 13:730–742, 2007. doi: 10.1016/j.devcel.2007.09.015.

[36] L. M. Escudero, F. Costa Lda, A. Kicheva, J. Briscoe, M. Freeman, and M. M. Babu. Epithelial organisation revealed by a network of cellular contacts. *Nat. Commun.*, 2:526, 2011. doi: 10.1038/ncomms1536.

[37] L. Legoff, H. Rouault, and T. Lecuit. A global pattern of mechanical stress polarizes cell divisions and cell shape in the growing *Drosophila* wing disc. *Development*, 140: 4051–4059, 2013. doi: 10.1242/dev.090878.

[38] O. Wartlick, F. Jülicher, and M. Gonzàlez-Gaitàn. Growth control by a moving morphogen gradient during *Drosophila* eye development. *Development*, 141:1884–1893, 2014. doi: 10.1242/dev.105650.

[39] H. F. Gómez, M. S. Dumond, L. Hodel, R. Vetter, and D. Iber. 3D cell neighbour dynamics in growing pseudostratified epithelia. *eLife*, 10:e68135, 2021. doi: 10.7554/eLife.68135.

[40] M. Saitoh, T. Shirakihara, A. Fukasawa, K. Horiguchi, K. Sakamoto, H. Sugiya, H. Beppu, Y. Fujita, I. Morita, K. Miyazono, et al. Basolateral BMP signaling in polarized epithelial cells. *PLoS One*, 8:e62659, 2013. doi: 10.1371/journal.pone.0062659.